

Read our COVID-19 research and news.



RESEARCH ARTICLE | NEUROIMMUNOLOGY

T cell engagement of cross-presenting microglia protects the brain from a nasal virus infection

 E. Ashley Moseman^{1,2,*†},  Alexa C. Blanchard^{1,*},  Debasis Nayak³ and  Dorian B. McGavern^{1,†}

+ See all authors and affiliations

Science Immunology 05 Jun 2020:
Vol. 5, Issue 48, eabb1817
DOI: 10.1126/sciimmunol.abb1817

Article

Figures & Data

Info & Metrics

eLetters

 PDF

Safeguarding the sense of smell

Given the proximity of the olfactory bulb to the upper airways, it is surprising that viruses that infect the upper airways, including influenza, rarely infect the brain. In mice, intranasal infection with vesicular stomatitis virus (VSV) does result in infection of sensory neurons in the olfactory bulb. Using VSV that expresses a fluorescent reporter, Moseman *et al.* examined the ability of VSV to infect distinct cell types within olfactory bulb. Although VSV infection was restricted to neurons within the olfactory bulb, they found that microglial cells that were not infected by VSV to be the key in priming T cell responses that promoted viral clearance.

Abstract

The neuroepithelium is a nasal barrier surface populated by olfactory sensory neurons that detect odorants in the airway and convey this information directly to the brain via axon fibers. This barrier surface is especially vulnerable to infection, yet respiratory infections rarely cause fatal encephalitis, suggesting a highly evolved immunological defense. Here, using a mouse model, we sought to understand the mechanism by which innate and adaptive immune cells thwart neuroinvasion by vesicular stomatitis virus (VSV), a potentially lethal virus that uses olfactory sensory neurons to enter the brain after nasal infection. Fate-mapping studies demonstrated that infected central nervous system (CNS) neurons were cleared

interfered with T cell calcium signaling and antiviral control in the brain after nasal infection. Collectively, these data demonstrate that microglia provide a front-line defense against a neuroinvasive nasal infection by cross-presenting antigen to antiviral T cells that noncytolytically cleanse neurons. Disruptions in this innate defense likely render the brain susceptible to neurotropic viruses like VSV that attempt to enter the CNS via the nose.

INTRODUCTION

Viral infections of the central nervous system (CNS) can be devastating when not properly contained (1, 2). Because the CNS contains irreplaceable postmitotic cells, it is protected by several physical barriers that limit pathogen access into the CNS, including the blood-brain barrier (BBB), blood cerebrospinal fluid barrier (BCSFB), and skull, among others. In addition, immune responses in this compartment are heavily regulated (3). Viruses, in turn, use several approaches to bypass these barriers such as direct infection of the BBB, invasion of peripheral nerves followed by transport into the CNS, and “trojan horse” entry via surveying immune cells (4). One especially vulnerable route that viruses use to invade the CNS is via olfactory sensory neurons (OSNs) within the nasal cavity.

OSNs lie within the mucosal upper airway surface, which is constantly exposed to environmental pathogens. However, the olfactory epithelium (OE) lining the nasal turbinates is unique in that this mucosal surface provides access for viruses to enter the CNS. Unlike the neighboring respiratory epithelium, the OE contains thousands to millions of OSNs (depending on the species) that are the predominant cell type within the olfactory neuroepithelial surface. Although the OSN cell bodies lie beneath a layer of supporting or sustentacular cells, they extend a ciliated dendrite into the mucus lined airway space. Odorant information gathered from the external environment is conveyed via OSN axons within the turbinates through the specialized cribriform plate at the front of the skull and into the olfactory bulb (OB) of the brain (5). However, this anatomical arrangement also results in OSNs serving as a direct single-cell route for neuroinvasion. Pathogens that infect OSNs can be shuttled intracellularly along OSN axons directly into the brain. The intracellular passage via OSNs into the brain allows invading pathogens to “tunnel under the castle wall” and evade classical CNS barriers that typically shield the brain. Thus, the olfactory route of infection is especially vulnerable to neurotropic viruses (6, 7).

The immune response to viruses must be appropriately balanced between pathogen clearance and limiting tissue damage. This balance is especially important in the CNS because most neurons are unable to regenerate, and damage can result in permanent damage to neural networks (1).

On the other hand, IFN γ , which is primarily produced by lymphocytes [CD8⁺, CD4⁺, and natural killer (NK) cells], plays a dominant role in the control of CNS viral infections (14–17). Tumor necrosis factor- α (TNF α) has also been shown to facilitate noncytolytic clearance (18–20).

Upper airway infections are a ubiquitous part of human life, and although many viruses infect the respiratory system (e.g., influenza, rhinovirus, coronavirus, and respiratory syncytial virus), several of these viruses can also infect the OE. In this study, we used vesicular stomatitis virus (VSV) as a model for nasal infection because of its ability to target the OE preferentially over the respiratory epithelium (21)—a preference shared by herpes simplex virus (HSV) (22). Several other viruses can also infect the OE, including mouse hepatitis virus (MHV) (23), parainfluenza (24), Japanese encephalitis virus (JEV) (25), and influenza virus (6, 26). Whereas seasonal influenza is typically an infection of respiratory epithelium (27), some more pathogenic strains are **clearly** able to target OSNs (26). Highly pathogenic avian influenza H5N1 prefers to replicate within the OE (28).

We undertook this study to better understand the mechanisms by which a cytopathic virus that infects the OE is contained and ultimately prohibited from spreading throughout the CNS. Intranasal VSV infection can induce a potent encephalitis that varies in outcome depending on the age and strain of the infected animal (29). After nasal infection, VSV is transported from the airway via the OE into the CNS, where it is initially observed within the OB (30). Virus replication is usually halted at the glomerular layer of the OB where OSN projections enter (10); however, the virus can sometimes move into deeper regions of the OB and throughout the CNS. VSV that escapes this OSN-glomerular junction is believed to use retrograde axon transport and the ventricular system to move caudally in the CNS (31). It is known that IFN-I (32, 33), B cells (33, 34), and antiviral T cells (29, 35) all play a role in containing VSV. In this study, we monitored the in vivo activities of CD8⁺ T cells in the anatomical site where VSV is typically contained within the OB (glomeruli) and probed for the most functionally relevant source(s) of antigen presentation that result in noncytolytic VSV control in neurons. Unexpectedly, an innate immune cell that is never infected by the virus (microglia) served as a key player in the control of virus in neurons.

RESULTS

Virus infection of the olfactory epithelial leads to rapid neuroinvasion

To more precisely understand how neurotropic viruses invade the CNS after infection of the OE, we inoculated mice intranasally with VSV expressing DsRed (VSV-DsRed). This approach enabled us to monitor the distribution and spread of the virus in olfactory tissue. Confocal imaging of coronal whole head sections (fig. S1) revealed 24 hours after intranasal infection that there was widespread

revealed that VSV was very efficient at gaining access to the brain via this intranasal route (**Fig. 1E**). Viral titers reached $\sim 10^4$ plaque-forming units (PFU) at 24 hours and climbed to $\sim 10^5$ PFU on day 6 before being extinguished by day 8.

[Download high-res image](#) | [Open in new tab](#) | [Download Powerpoint](#)

Fig. 1 VSV rapidly travels from the nasal turbinates into the OB where it is controlled noncytolytically.

(**A** and **B**) Representative confocal micrographs of coronal head sections (see fig. S1) show the nasal airway, OE, cribriform plate (white dotted line), and OBs from OMP-GFP mice on days 1 (**A**) and 6 (**B**) after intranasal VSV-DsRed (green) infection (OMP-GFP in red, nuclei shown in blue). (**C** and **D**) Higher magnification images show the virus invading the OE at day 1 (**C**) and OB via the outer nerve layer at day 6 (**D**). Anatomical structures such as the airway, OE, olfactory nerve layer (ONL), glomerular layer (GL), and mitral cell layer (MCL) are annotated in these images. (**E**) Time course of viral titers represented as PFU per OB after intranasal VSV infection (means \pm SD; $n = 4$ to 5 mice per time point; data representative of three independent experiments). (**F**) Confocal micrographs of a cleared OB from a VSV-iCre infected Stop^{fl/fl} tdTomato reporter mouse 50 days after intranasal infection.

To protect the CNS, noncytolytic viral clearance is often favored in this compartment (**36**). However, because VSV is a cytopathic virus, it was unclear whether this lifecycle could be halted once initiated. To determine whether a cytopathic virus could be cleared noncytolytically from the brain, we generated a recombinant of VSV expressing iCre-recombinase (VSV-iCre). We then conducted fate-mapping studies by infecting floxed Stop TdTomato reporter (Stop^{fl/fl} TdTomato) mice with this recombinant virus. We observed dense patches TdTomato⁺ cells with a definitive neuronal morphology in the OB at late time points (>40 days) (**Fig. 1F** and fig. S2), long after infectious virus was cleared from this compartment (**Fig. 1E**). These data indicate that VSV can be noncytolytically cleared from the OB, although it does not exclude the possibility that some cells are cytolytically cleared as well.

Intranasal VSV infection induces a robust immune response in the olfactory system

Except for patches of bone marrow within the turbinate bones, the naïve OE as shown in coronal head sections (fig. S1A) contains few hematopoietic cells (**Fig. 2A**); however, after nasal infection, widespread VSV replication within the OE provoked robust inflammatory cell infiltration. CD45⁺ leukocytes were observed in the OE as early as day 2, and infiltration elevated massively by day 6

[Download high-res image](#) | [Open in new tab](#) | [Download Powerpoint](#)

Fig. 2 Intranasal VSV infection drives massive immune cell infiltration into the OE and OB.

(A) Representative confocal images of coronal head sections (see fig. S1) show the distribution of CD45⁺ leukocytes (red) in OE/OB-uninfected mice relative to days 2 and 6 after intranasal VSV-GFP (green) infection. Cell nuclei are shown in blue. (B) Confocal micrograph depicting CD45⁺ infiltration into the VSV-eGFP-infected olfactory turbinates 6 days after infection. Note that the airway space denoted with white asterisk and white dotted lines is filled with cells and virus. (C) A confocal micrograph from a day 6 infected OB shows VSV-GFP in the glomerular layer (GL) and outer nerve layer (ONL). (D) Confocal micrograph of day 6 VSV-eGFP-infected OSN terminals. Asterisks denote individual glomeruli within the OB. (E) Graph depicts the kinetics of inflammatory cell infiltration into the VSV-infected OB. The following markers were used to identify the different immune subsets after first gating on living, CD45⁺ cells: neutrophils (Ly6C^{int}, Ly6G^{hi}, CD11b⁺) and monocytes (Ly6C^{hi}, CD11b^{hi}); NK cells (NK1.1⁺, TCRβ^{neg}), CD4 T cells (TCRβ⁺, CD4⁺, CD8⁻), and CD8 T cells (TCRβ⁺, CD4⁺, CD8⁻) (means ± SD; *n* = 4 to 5 mice time point; data representative of three independent experiments). (F) Kinetics of adoptively transferred antigen-specific CD8⁺ OT-I T cell expansion in the OB, draining mandibular and superficial cervical LNs, and spleen after intranasal VSV infection. OT-I cells were defined as living, CD45.1⁺, CD8⁺, mTomato⁺ (means ± SD; *n* = 4 to 5 mice per time point; two independent experiments).

Under steady state, the OB is defended in part by resident microglia; however, the arrival of VSV into this compartment via OSNs is associated with a large influx of peripherally derived immune cells that surrounded infected glomeruli (**Fig. 2, A and C to E**). This response was dominated by neutrophils and NK cells during the first 3 days, which were superseded by CD8⁺ T cells and Ly6C^{hi} monocytes at day 6 after infection (**Fig. 2E**). CD4⁺ T cells also arrived at this time point. At day 8 after infection, T cell and monocyte numbers increased further within the OB (**Fig. 2E**). To track the recruitment of virus-specific CD8⁺ T cells to the OB, we seeded mice intravenously with 3000 mCerulean⁺ OT-I and then infected them intranasally with VSV–ovalbumin (OVA). VSV-specific CD8⁺ T cells were primed and proliferated in the draining cervical lymph nodes and spleen and increased steadily over time in the OB (**Fig. 2F**). These data demonstrate that the OB mounts a robust immunological defense against intranasal VSV infection.

T cells and antiviral effector molecules protect against fatal VSV encephalitis

VSV titers in the OB are controlled between days 6 and 8 after infection (**Fig. 1E**), which coincided with the arrival of antiviral T cells (**Fig. 2, E and F**). We therefore sought to better understand the role of these T cells in preventing the fatal spread of VSV from olfactory glomeruli throughout the brain. We used survival rather than viral titers as an initial screen because we wanted to identify

observation, we found increased viral titers in the OB (**Fig. 3B**) and caudal brain (**Fig. 3C**) of T cell-depleted mice at day 8 after infection. In addition, although VSV–green fluorescent protein (GFP) was largely confined to the outer nerve layer and glomeruli of control mice (**Fig. 3, D and F**), T cell depletion promoted movement of VSV-GFP to other brain regions, including the rostral migratory stream and brainstem (**Fig. 3, D and F**). T cell depletion also allowed VSV-GFP to invade deeper layers of the OB, such as the mitral cell layer (**Fig. 3E**).

[Download high-res image](#) | [Open in new tab](#) | [Download Powerpoint](#)

Fig. 3 T cells prevent fatal VSV neuroinvasion after intranasal infection.

(**A**) Survival curves of isotype control, α CD4-, α CD8-, or α CD8/ α CD4-treated mice after intranasal VSV infection ($n = 28$ mice for isotype; $n = 10$ for α CD4 depleted, $P = 0.0183$; $n = 11$ for α CD8 depleted, $P = 0.0263$; $n = 31$ mice for α CD8/4 depleted, $P < 0.0001$; two independent experiments). (**B and C**) Viral titers from the OB (**B**) and remaining cerebrum (**C**) of isotype control or T cell-depleted mice 8 days after intranasal VSV infection ($n = 4$ mice per group; two independent experiments; $*P = 0.0286$, $**P = 0.008$). Black lines denote means \pm SD. (**D**) Representative confocal micrographs of sagittal brain sections (see fig. S1B) from an isotype control (left) or T cell-depleted mouse (right) 8 days after intranasal VSV-eGFP infection. (**E**) Representative confocal micrographs of viral escape from the glomerular layer within T cell-depleted OBs after VSV-eGFP infection. (**F**) Quantification of VSV-eGFP signal in the forebrain and hindbrains of isotype control or T cell-depleted animals ($n = 8$ per group; three independent experiments; $*P = 0.02$). Black lines denote means \pm SD. (**G**) Survival curves for VSV-OVA-infected control, antibody-treated mice, and genetically deficient mouse strains ($n = 40$ mice for control; $n = 20$ for $\text{TNF}\alpha^{-/-}$, $P < 0.0021$; $n = 9$ for $\text{IFNAR}^{-/-}$, $P < 0.0001$; $n = 20$ for $\text{IFN}\gamma^{-/-}$, $P = 0.02$; $n = 23$ for $\text{PRF1}^{-/-}$; $P = 0.1039$; data are pooled from six independent experiments). (**H**) Survival curves for control and floxed $\text{IFN}\gamma\text{R}$ mice infected intranasally with VSV-iCre ($n = 10$ mice for control; $n = 9$ mice for floxed $\text{IFN}\gamma\text{R}$; $P = 0.3657$; two independent experiments).

We next examined the effector mechanisms involved in preventing fatal VSV encephalitis. Mice deficient in $\text{TNF}\alpha$, $\text{IFN}\gamma$, or perforin (PRF1) all showed modest reductions in survival comparable with that observed in mice depleted with anti-CD8 or CD4 antibodies (**Fig. 3G**). None of these knockout mice phenocopied the incidence of fatal disease observed in mice receiving anti-CD8/4-depleting antibodies (**Fig. 3A**). To determine whether expression of the $\text{IFN}\gamma\text{R}$ was required on infected cells, we inoculated floxed $\text{IFN}\gamma\text{R}$ with VSV-iCre (**Fig. 3H**). This, however, did not reduce survival, indicating that $\text{IFN}\gamma\text{R}$ is not required on infected cells to elicit antiviral control. Collectively, these data suggest that there are redundant effector mechanisms controlling VSV within the OB.

VSV-specific versus bystander CD8⁺ T cell dynamics in the living OB at day 6 or 7 after infection. We selected these time points because viral titers in the OB declined rapidly between days 6 and 8 after infection (**Fig. 1E**), and we wanted to understand the mechanism by which this occurred. One day before VSV-OVA infection, B6 mice were seeded with 3000 mCerulean⁺ OT-I cells that served as the virus-specific CD8⁺ T cell population. Bystander cells were generated by seeding a separate group of B6 mice with orange fluorescent protein–positive (OFP⁺) P14 cells, which are specific to the glycoprotein of lymphocytic choriomeningitis virus (LCMV) (**37**). These mice were then infected intraperitoneally with LCMV Armstrong, and at day 7, effector OFP⁺ P14 cells were harvested from the spleen and transferred into VSV-GFP-OVA–infected mice 1 day before imaging. mCerulean⁺ OT-I (VSV-specific) and OFP⁺ P14 (bystander) cells were imaged simultaneously by intravital two-photon microscopy (TPM) through a thinned skull preparation (**38, 39**) made above the OB. This technique allowed us for the first time to analyze antiviral T cell behavior in the virally infected OB. After VSV-GFP-OVA infection, virus-specific CD8⁺ T cells moved rapidly along, between, and across infected axon tracts in the outer nerve layer and within the glomeruli (**Fig. 4, A and B**, and movies S1 and S2). Quantification of T cell track velocities in two-photon time lapses revealed that virus-specific CD8⁺ T cells had reduced track velocities relative to bystander T cells imaged in the same OB (**Fig. 4, C and D**). In addition, virus-specific CD8⁺ T cells also had a lower motility coefficient and higher arrest coefficient (**Fig. 4D**), all suggesting that these cells were encountering antigen locally (**40**).

[Download high-res image](#) | [Open in new tab](#) | [Download Powerpoint](#)

Fig. 4 Antiviral CTLs exhibit decreased motility within the virally infected OB.

(**A**) Representative image from an intravital imaging experiment depicting adoptively transferred virus-specific OT-I T cells (cyan) within the VSV-GFP (green)–infected OB glomerular layer at day 7 after infection. (**B**) Representative image from a two-photon imaging experiment showing VSV-specific OT-I T cells (blue) and LCMV-specific P14 T cells (red) traveling along VSV-eGFP (green)–infected nerve fibers in the OB outer nerve layer. Mice were coinfecting with VSV-eGFP and VSV-OVA for this experiment. (**C**) Mean track velocity of VSV-specific OT-I T cells and LCMV-specific P14 T cells in day 7 VSV-infected OB ($n = 4$ mice; 305 OT-I T cells and 57 P14 T cells; **** $P < 0.0001$). Colored horizontal lines denote means \pm SD. (**D**) Motility analysis comparing average track velocities, arrest coefficients, and motility coefficients for VSV-specific OT-I T cells relative to bystander LCMV-specific P14 T cells within the infected OB at day 7 (from the same experiments as above; $n = 4$ mice; average velocity, $P < 0.0001$; arrest coefficient, $P = 0.003$; motility coefficient, $P < 0.0001$).

fluorescent calcium concentration indicator protein (13). Six days after intranasal infection with VSV-OVA, calcium flux was visible in virus-specific CD8⁺ T cells that had infiltrated and were surveying the OB (Fig. 5, A, B, and D, and movie S3). Calcium flux was rarely observed in infiltrating bystander P14 CD8⁺ T cells, indicating that T cell calcium flux is a good surrogate for cognate peptide MHC recognition (Fig. 5B) (13). We also observed that calcium fluxing virus-specific OT-I CD8⁺ T cells had reduced instantaneous velocities relative to the cells that were not fluxing (Fig. 5C), which is consistent with studies showing that T cell antigen recognition is associated with decreased motility (40).

[Download high-res image](#) | [Open in new tab](#) | [Download Powerpoint](#)

Fig. 5 Antiviral CTLs engage antigen on an uninfected CNS-resident cell type.

(A) A representative image from a two-photon imaging experiment shows OT-I mTomato⁺ GCaMP6s⁺ T cells in day 6 VSV-OVA infected OB. (B) Calcium flux frequency of VSV-specific OT-I mTomato⁺ GCaMP6s⁺ T cells compared with calcium flux frequency in bystander LCMV-specific P14 mTomato⁺ GCaMP6s⁺ T cells within VSV-OVA-infected OB ($n = 4$ mice; six time periods sampled per mouse; 24 OT-I T cells, 20 P14 T cells; **** $P < 0.0001$). Colored horizontal lines denote means \pm SD. (C) Mean velocities of calcium fluxing versus non fluxing OT-I mTomato⁺ GCaMP6s⁺ T cells within VSV-OVA-infected OB ($n = 3$ mice; 39 OT-I T cells; **** $P < 0.0001$). Colored horizontal lines denote means \pm SD. (D) A representative time lapse from an intravital imaging experiment shows two different OT-I⁺ mTomato⁺ GCaMP6s⁺ T cells fluxing calcium (green) upon interaction with autofluorescent cells (yellow) within the VSV-OVA-infected OB at day 6. The white arrow denote a T cell engaged in a kinetic fluxing behavior, whereas the cyan arrowhead denote a stably arrested T cell fluxing calcium. (E) Calcium and motility profiles for representative OT-I kinetic (top, velocity of $>2 \mu\text{m}/\text{min}$) and stable (bottom, $<2 \mu\text{m}/\text{min}$) interactions. (F) Frequency of kinetic and stable calcium flux events in virus-specific OT-I T cells within the OB 6 days after VSV-OVA infection [$(n = 4$ mice; 99 OT-I T cells total: 64 kinetic ($>2 \mu\text{m}/\text{min}$) and 35 stable ($<2 \mu\text{m}/\text{min}$)]. (G) Number of calcium flux events as a function of velocity during kinetic and stable virus-specific OT-I T cells interactions in OB at day 6 ($n = 4$ mice; 99 OT-I T cells total, same as above; $P = 0.001$). (H) Calcium flux frequency of OT-I mTomato⁺ GCaMP6s⁺ T cells within WT nonchimeric, control bone marrow chimeric, and MHC I-deficient bone marrow chimeric mice ($n = 4$ mice; 6 time points sampled per movie; **** $P < 0.0001$). Horizontal lines denote means \pm SD. (I) Survival curves for WT ($n = 33$ mice), floxed $\beta_2\text{M}$ ($n = 19$ mice), and αCD8 depleted WT mice ($n = 13$ mice) intranasally infected with VSV-iCre ($P = 0.0016$ for WT versus αCD8 , $P = 0.2825$ for WT versus $\beta_2\text{M}$, $P = 0.0347$ floxed $\beta_2\text{M}$ versus αCD8).

We next classified virus-specific CD8⁺ T cell interactions in the virally infected OB into two groups based on velocity. “Kinetic” interactions were defined by continued T cell motility while fluxing

cell would fully arrest and then flux calcium; however, this was only observed in 35% of the antigen encounters (**Fig. 5, E and F**, and movie S3). Stable interactions typically resulted in more calcium fluxes (**Fig. 5G**) and longer flux durations relative to the kinetic interactions (fig. S3).

Having defined the dynamics of virus-specific CD8⁺ T cell interactions in the infected OB, we next sought to define target cell identity. In our imaging studies, we often noted that T cells would flux calcium upon engagement of “autofluorescent” cells (**Fig. 5, A and D**, and movie S3). Morphologically, these autofluorescent cells did not match the size, shape, or spatial distribution of VSV-GFP infected cells that we typically observed in the OB. Because hematopoietic cells massively infiltrated the OB after VSV infection (**Fig. 2**), we posited that an infiltrating cell population might be responsible for presenting local antigen to virus-specific CD8⁺ T cells. To address this possibility, we generated bone marrow chimeras in which the CNS-resident compartment lacked MHC I, whereas the infiltrating hematopoietic compartment was MHC I sufficient. The percentage of donor-derived hematopoietic cells in the blood of these mice was $99.2 \pm 0.4\%$, demonstrating near-complete chimerism. The overall frequency of cytotoxic lymphocyte (CTL) calcium flux dropped significantly in mice lacking MHC I on the CNS-resident compartment, indicating that antigen presentation to virus-specific CD8⁺ T cells relied primarily on a radiation-resistant brain cell population rather than infiltrating hematopoietic cells (**Fig. 5H**). VSV is known to infect neurons, but MHC I is expressed at very low levels on these cells (**43, 44**). We nevertheless set out to evaluate the importance CTL-neuronal interactions in controlling an intranasal VSV infection. To address this question, we generated a conditional β_2 -microglobulin (β_2 M) mouse in which the exons 2 and 3 are flanked by loxP sites (floxed β_2 M) (fig. S4A). β_2 M is an essential component of the MHC I surface complex, and thus, removal severely impairs presentation of class I peptides (**45**). We infected “conditional β_2 M” mice with VSV-iCre to remove the possibility that infected cells engage in direct antigen presentation to CD8⁺ T cells. Infection with VSV-iCre resulted in deletion of β_2 M from the genome of infected cells (fig. S4B). However, unexpectedly, VSV-iCre–infected floxed β_2 M mice survived intranasal infection at the rate of control animals (**Fig. 5I**), indicating that the antiviral pressure exerted by CD8⁺ T cells, which is required in part for survival, does not involve direct interactions with virus-infected cells.

Microglia within the infected OB are activated and present antigen to CTLs

Microglia are radiation-resistant CNS-resident myeloid cells, and although they are not believed to be potent antigen-presenting cells in the naïve state (**46**), we characterized the surface expression of antigen-presenting molecules on microglia during VSV infection (**Fig. 6, A and B**). Six days after VSV infection, microglia in the OB showed evidence of activation characterized by robust up-regulation of MHC I, CD80, and CD86 as well as a very modest increase in CD40 and MHC II

Fig. 6 Microglia elicit antigen-specific calcium flux from antiviral CTLs.

(A) Representative flow cytometric histograms of OB microglia show surface molecule expression 6 days after VSV infection (red) compared with naïve OB microglia (gray). Microglia were defined as Thy1.2⁻, CD11b⁺, Ly6C⁻, Ly6G⁻, and CD45^{int}. (B) Quantification of surface molecule geometric mean fluorescent intensity (GMFI) on OB microglia 6 days after VSV infection versus naïve OB microglia. GMFI data for each surface marker are plotted as the means \pm SD after subtracting the isotype control antibody GMFI ($n = 4$ mice per group; two independent experiments; * $P < 0.05$, ** $P < 0.01$, **** $P < 0.0001$). (C) Pie chart representing the frequency of all VSV-specific OT-I T cell calcium flux events observed by TPM in contact or not in contact with CX3CR1^{gfp/+} OB microglia in day 6 after VSV-OVA-infected bone marrow chimeric mice (i.e., CX3CR1^{gfp/+} mice with C57BL/6J bone marrow) ($n = 5$ mice; 9 movies; 61 time points; four independent experiments: $P < 0.0001$). (D) A representative time lapse from a two-photon imaging experiment shows an OT-I mTomato⁺ GCaMP6s⁺ T cells in a day 6 VSA-OVA-infected CX3CR1^{gfp/+} bone marrow chimera. Arrows (white and cyan) denote two virus-specific OT-I T cells fluxing calcium upon engagement of a single CX3CR1^{gfp/+} microglia (black asterisks) in the infected OB.

We next sought to directly observe in vivo whether microglia were presenting antigen to virus-specific CD8⁺ T cells. To accomplish this, we adoptively transferred naïve mTomato⁺ GCaMP6s⁺ OT-I cells into bone marrow chimeras in which CX3CR1^{gfp/+} were reconstituted with wild-type (WT) bone marrow ($99.6 \pm 0.31\%$ blood chimerism). In these chimeras, radioresistant microglia are GFP positive, whereas all peripherally derived hematopoietic cells as well as perivascular and meningeal macrophages are GFP negative. Six days after intranasal infection with VSV-OVA, we used intravital microscopy to identify calcium flux induced by antiviral CD8⁺ T cell engagement in the OB (movie S4). We then quantified the frequency of CD8⁺ T cell antigen recognition (calcium flux) occurring in contact with microglia versus unlabeled space within the OB. This study revealed that ~72% of CD8⁺ T cell calcium flux occurred in contact with a CX3CR1^{gfp/+} microglia (Fig. 6, C and D, and movie S4), suggesting that microglia are indeed presenting cognate peptide MHC I complexes to virus-specific T cells. The interaction partner for the remaining CTL calcium flux events (~28%) is not known; however, we noted that the within the OB of the bone marrow chimeras, $23.4 \pm 3.9\%$ of the microglia were nonfluorescent (i.e., donor-derived). These cells might also have induced T cell calcium flux.

Microglia acquire infected OSN debris and orchestrate neuroprotective CTL activity

Our calcium imaging data suggested that microglia play an important role in presenting antigen to antiviral CD8⁺ T cells after VSV neuroinvasion. Neurons are the only known target of VSV after nasal infection; however, we decided to evaluate whether microglia were also infected. We sought

In the absence of direct microglia infection led us to investigate alternative mechanisms of antigen acquisition and presentation by microglia. VSV can cause damage to the neurons it infects, and microglia are known to phagocytose cellular debris. We therefore evaluated whether microglia acquired antigen from VSV-infected OSNs. We labeled OSNs within the OE by injecting fluorescent cholera toxin B (CTB) intranasally into olfactory marker protein-GFP (fig. S5C) or CX3CR1^{gfp/+} mice (**Fig. 7A**) (47). Ten hours later, after CTB was transported along OSN axons into OB glomeruli (fig. S5C), we infected mice with VSV and, 6 days later, observed evidence of CX3CR1^{gfp/+} cells with intracellular CTB obtained from the labeled OSNs (**Fig. 7A**). These cells had the morphological characteristics of microglia, and this was confirmed flow cytometrically, which revealed that ~5% of microglia in the OB contained CTB (i.e., OSN debris) 6 days after infection (**Fig. 7, B and C**). Processing the entire OB for flow cytometry, however, did not allow us to specifically analyze the anatomically relevant microglia in the glomerular layer of the OB, which is where VSV (**Fig. 2C**) and CTB (fig. S5C) enter via OSN axons. We therefore quantified uptake histochemically, allowing us to focus on this anatomical site. We found 6 days after VSV infection that ~40% of Iba-1⁺ myeloid cells in OB glomeruli contained intracellular CTB derived from OSNs (**Fig. 7D**). For these studies, CTB served as a surrogate for an OSN-derived antigen. We next wanted to address whether microglia could also acquire virus particles. This was accomplished by infecting mice with VSV-PeGFP—a viral recombinant in which the phosphoprotein (P) is fused to enhanced GFP (eGFP) enabling detection of the virion itself (48). Six days after infection with VSV-PeGFP, we determined that ~10% of Iba-1⁺ myeloid cells in OB glomeruli contained VSV-PeGFP (**Fig. 7E**). Collectively, these data indicate that microglia can directly acquire antigens from virally infected OSNs.

[Download high-res image](#) | [Open in new tab](#) | [Download Powerpoint](#)

Fig. 7 Microglia acquire and present antigen from virus-infected neurons to drive protective antiviral CTL responses.

(A) Representative confocal micrographs of OB microglia (green) containing fragments of OSNs labeled with CTB (white) 10 hours before VSV infection. Images were captured at day 6 after infection. (B) Representative fluorescence-activated cell sorting plots of microglia (Thy1.2⁻, Cd11b⁺, Ly6C/G⁻, and CD45^{int}) from CTB-treated control (top) or day 6 VSV-infected mice (bottom). (C) Quantification of CTB containing microglia frequencies. Values are normalized to VSV-infected mice without CTB to control for autofluorescence (7 mice per group; two independent experiments; *****P* < 0.001). Horizontal lines denote means ± SD. (D) Frequency of microglia containing CTB within the OB glomerular layer of day 6 VSV-infected mice as determined by quantification of confocal images. Values are normalized to VSV-infected mice without CTB to control for autofluorescence (*n* = 4 mice per group; *n* = 17 fields for day 6, seven fields for naïve; *****P* < 0.001). Horizontal lines denote means ± SD. (E) Frequency of GFP⁺ microglia within the OB glomerular layer 6 days after VSV-PeGFP infection as determined

CX3CR1-CreER x ROSA Stop^{fl/fl} DTR microglia-depleted animals as a function of microglia depletion efficiency (Pearson's $r = 0.753$, $P < 0.0013$). (H) Viral titers in the brains of control versus PLX3397-treated animals on day 7 after VSV infection (14 mice per group from three pooled independent experiments; $*P = 0.0265$). Horizontal lines denote means \pm SD. (I) Survival curve for control versus PLX3397-treated VSV-infected mice ($n = 36$ mice for control; $n = 35$ mice for PLX3397; $P = 0.0201$).

Having demonstrated that microglia could acquire OSN-derived antigens in vivo, we next asked whether their specific removal affected cognate antigen recognition of virus-specific CD8⁺ T cells in the infected OB. To deplete microglia, we first generated CX3CR1-Cre-ER x Rosa Stop^{fl/fl} diphtheria toxin receptor (DTR) mice and treated them with tamoxifen to drive DTR expression in myeloid cells. After tamoxifen cessation, we waited an additional 60 days before DT treatment to allow for peripheral monocyte turnover (49). This is a commonly used approach that allows microglial depletion while preserving CX3CR1-expressing monocytes and antiviral T cells. These mice were then seeded with naïve mTomato⁺ GCaMP6s⁺ OT-I cells and infected intranasally with VSV-OVA. Six days later, we observed that virus-specific CD8⁺ T cell calcium flux was significantly reduced in the microglia-depleted mice (Fig. 7F), indicating compromised viral antigen presentation when OB microglia but not monocytes were reduced (fig. S6, A and B). Because the microglia depletion efficiency varied between animals, we tested whether there was any relationship between the frequency of CD8⁺ T cell calcium flux and the percentage of microglia remaining in the OB. We observed a strong positive correlation ($r = 0.75$, $P < 0.0013$) between these two variables, further emphasizing the importance of microglia in fostering cognate antigen recognition and calcium flux in antiviral CD8⁺ T cells (Fig. 7G).

Last, we assessed the degree to which microglia contributed to the antiviral defense against an intranasal VSV infection. For this study, we used a more convenient alternative method to deplete microglia. Specifically, C57BL/6J mice were fed chow containing the CSF1R antagonist pexidartinib (PLX3397) for 1 month (50). This treatment decreased the number of microglia in the OB by 66% without reducing the recruitment of CD8⁺ or CD8⁺ OT-I T cells in day 7 VSV-OVA-infected mice (fig. S6). Despite the preservation of CD8⁺ T cells, VSV infection of PLX3397-treated animals resulted in frequent viral escape at day 7 after infection with elevated brain viral titers compared with control animals (Fig. 7H). Moreover, viral escape in PLX3397-treated mice was accompanied by reduced survival (Fig. 7I), which mirrored that observed in mice depleted of CD8⁺ T cells (Fig. 3G). Collectively, these data suggest that microglia can acquire and cross-present locally derived viral antigen to brain-infiltrating CD8⁺ T cells that exert antiviral pressure and contain VSV in the OB.

it enters and attempts to spread throughout the CNS. Nasal VSV infection induced massive leukocyte infiltration into the OE. The virus nevertheless managed to travel via OSN axons through the cribriform plate and into the OB. Within the OB, fate-mapping studies revealed that VSV was controlled noncytolytically after infecting neurons in glomeruli as well as deeper neuronal layers. This containment depended in part on antiviral T cells and a combination of effector molecules (perforin, IFN γ , TNF α). However, specific removal of MHC I from virus-infected cells using floxed β_2 M mice demonstrated that direct engagement of neurons by CD8⁺ T cells was not required for viral control. This unexpected observation led us to perform intravital imaging studies of cognate antigen recognition by virus-specific CD8⁺ T cells in infected glomeruli. These studies revealed that microglia displayed cognate peptide-MHC I, promoting CTL antigen recognition and calcium flux. Microglia were not infected by VSV but instead acquired antigen from adjacent neurons, which was then cross-presented to the infiltrating virus-specific CTLs. These interactions were functionally important, because microglia depletion markedly reduced cognate antigen recognition by CTLs, impeding viral containment within the OB and promoting the development of fatal encephalitis.

After nasal inoculation, virus is rapidly transported from the airway via the OSNs into the CNS where it is seen primarily within the OB. Viral replication is usually halted at the OSN-glomerular junction (10). Previous studies have shown that T cells play an important role in the control and clearance of VSV after CNS infection (29, 35). In addition, IFN γ , TNF α , interleukin-12, and nitric oxide synthase 1 were all shown to participate in the antiviral defense against VSV (51–55), yet it is presently unclear how T cell effector functions are regulated in the CNS. Regulation of T cell effector functions is important because adult neurogenesis is reserved for specialized compartments [such as the OE (56, 57)]; thus, when neurons are lost in the CNS during adulthood, they typically are not replaced. Because of this, it is postulated that the CNS favors the use of noncytolytic viral clearance—a well-described cytokine-mediated mechanism of eradicating an intracellular pathogen without killing the cell (18, 58). Cytokines such as IFN γ , TNF α , and IFN-I are all capable of purging viruses noncytolytically, and this mode of viral clearance has been described for many different pathogens, including hepatitis B virus (59), LCMV (60, 61), influenza virus (62, 63), MHV (64), and Sindbis virus (65).

VSV is a cytopathic pathogen that is highly lytic in vitro (66); however, its interaction with the CNS appears to be more nuanced, as mice infected with VSV can sometimes harbor virus for several weeks before succumbing (Fig. 3A). Although we cannot exclude a role for CTLs using cytolytic effector molecules like perforin to control this virus (Fig. 3G), our fate mapping studies in VSV-iCre–infected Stop^{fl/fl} TdTomato reporter mice revealed ample evidence of previously infected OB neurons that were cleared noncytolytically. These results are consistent with a previous study showing that

known to help control measles virus (14), herpes virus (16), MHV (67), Borna virus (68), and recombinant vaccinia virus (69), whereas TNF α has a protective role against West Nile virus (WNV) (70), JEV (71), tick-borne encephalitis virus (72), and HSV (73). In our study, VSV-iCre allowed us to distinguish the direct effects of IFN γ on infected cells from other potential functions exerted by this cytokine, such as the activation and recruitment of immune cells (74–76). We observed that IFN γ R expression by infected cells plays no direct antiviral role in mediating survival after intranasal VSV inoculation. Whether TNF receptor is required on infected cells in this model is presently unclear.

MHC I is important for different phases of normal brain development and for controlling ongoing plasticity (77, 78). However, MHC I expression is often undetectable on most CNS neurons (43, 44, 79), and its ability to engage in physiologically relevant levels of antigen presentation is a source of continued debate. The classical paradigm suggests that activated CTLs enter virally infected tissues and recognize cognate viral peptides presented in MHC I molecules displayed on the infected cell surface. After some viral infections, neuronal MHC I does appear to play a role in containing virus through CTL pressure, and these interactions can facilitate release of immune effector molecules and eventual neuronal damage (80). During HSV infection, CTL-derived IFN γ is believed to contribute to noncytolytic maintenance of viral latency within infected neurons (16, 81). In addition, perforin and granzyme B also participate in the noncytolytic control of this virus in neurons by degrading the HSV-1 immediate early protein (82). By contrast, CNS neurons infected by WNV are believed to be targeted directly by CTLs that use perforin-mediated cytolytic mechanisms to purge virally infected neurons (83). It is presently unclear why some CTL engagements of infected neurons result in cytopathology, whereas others do not. This could be linked to the amount of MHC I expressed by different neuronal subtypes.

Although CTLs have the capacity to engage at least some virus-infected neuronal populations, our results in VSV-iCre–infected floxed β_2 M mice demonstrate that MHC I expression on infected neurons does not play a role in protecting mice from fatal encephalitis (Fig. 5I). CTLs are, however, important in preventing fatal disease after intranasal VSV infection (Fig. 5I), and our intravital imaging studies of cognate antigen recognition by antiviral CTLs in the OB uncovered that microglia served as the target of at least 70% of these interactions. This was especially unexpected because we found no evidence, using two sensitive methods, that microglia were infected by VSV (fig. S5A and B). These results suggested that microglia were, in fact, acquiring antigen from adjacent neurons and cross-presenting the material via MHC I to CTLs. This conclusion is supported by our data showing that microglia within the OB engulfed the neuronal tracer CTB and fluorescent protein–tagged VSV particles—a process that supplies potentially cross-presentable MHC I antigen. Cross-presentation is thought to be important during naïve CTLs priming within secondary lymphoid

immunopathology after CNS virus infection (80–93). Depletion studies have revealed that microglia participate in the antiviral defense against pseudorabies virus (88), JEV (87), MHV (89), Theiler's murine encephalomyelitis virus (90), VSV (91), and WNV (87, 92). For example, Wheeler *et al.* (89) found that many microglia-depleted mice fail to control MHV, resulting in compromised survival after intracerebral infection. This study also noted that microglia-depleted animals had impaired CD4⁺ T cell accumulation and function within the CNS. This is noteworthy because unlike microglia from VSV-infected brains (Fig. 6A) (94), MHV infection induces a marked up-regulation of MHC II on microglia. These two models of virus infection appear to showcase an important functional divergence in the ability of microglia to support either MHC I- or MHC II-restricted T cell responses in the virally infected CNS. The importance of separating MHC I and II presentation to effector T cells in the CNS is not known; however, this is the case after VSV infection, because OB-infiltrating myeloid cells express very high levels of MHC II, whereas microglia do not (94).

Although we did not focus on virus-specific CD4⁺ T cell interactions in this study, our findings demonstrate a role for cross-presenting microglia in displaying cognate peptide–MHC I complexes to CTLs. We had intended to provide a more direct role for MHC I expression on microglia by conditionally deleting β_2M from these cells. However, VSV infection of CX3CR1-Cre-ER × floxed β_2M mice resulted in near-complete NK cell-mediated deletion of the MHC I class negative microglia similar to what was described previously in inflamed floxed β_2M mice (95). Nevertheless, our intravital imaging studies revealed that microglia supported most of the CTL calcium flux activity in the OB, and cognate antigen recognition was markedly reduced in their absence. CTL calcium flux in the infected OB correlated positively with the number of microglia remaining in depleted mice. In addition, microglia depletion promoted both viral escape into the brain and increased the incidence of fatal encephalitis. Antigen presentation by uninfected microglia to infiltrating CTLs is likely a mechanism the CNS uses to elicit antiviral activity but protect neurons from direct CTL contact and potential lysis. It is also important to note that most CTL interactions with microglia were short lived (kinetic) rather than stable. It is postulated that these short-lived interactions favor CTL usage of antiviral molecules (e.g., cytokines) rather than killing behavior (42). This would provide a mechanism to control virus in adjacent neurons without engaging them.

In conclusion, this study relied on intravital microscopy to analyze cognate antigen recognition by CTLs as a nasal virus attempted to enter the brain via infection of the peripheral nervous system (i.e., OSNs). Because VSV primarily infects neurons, it was unclear how CTLs would exert their antiviral pressure on a cell population that expresses little to no MHC I. However, our studies uncovered cross-presenting microglia as the main innate immune cell type responsible for driving protective, noncytolytic CTL responses against a cytopathic CNS viral infection. These findings have

neurons by CTLs and favor release of noncytolytic antiviral cytokines through interactions with cross-presenting intermediaries. Microglia play an important role in synaptic pruning and CNS homeostasis, and their proximity to neurons makes them an ideal candidate for this task. Given the role of microglia in cross-presenting viral antigen, factors that result in their distraction or depletion are likely to render the CNS more susceptible to infection.

MATERIALS AND METHODS

Mice

C57BL/6J (B6), B6.129(Cg)-Gt(ROSA)26Sor^{tm4}(ACTB-tdTomato,-EGFP)^{Luo}/J (mTomato), C57BL/6-Tg(TcraTcrb)1100Mjb/J (OT-I), C57BL/6-Prf1^{tm1Sdz}/J (PRF^{-/-}), B6.Cg-Gt(ROSA)26Sor^{tm14}(CAG-tdTomato)Hze/J (Stop^{fl/fl} TdTomato), B6.129P2(Cg)-Cx3cr1^{tm2.1}(cre/ERT2)^{Litt}/WganJ (CX3CR1-Cre-ER), C57BL/6-Gt(ROSA)26Sor^{tm1}(HBEGF)^{Awai}/J (ROSA Stop^{fl/fl} DTR), C57BL/6N-Ifngr1^{tm1.1Rds}/J (IFNR^{fl/fl}) B6.129P-Cx3cr1^{tm1Litt}/J (CX3CR1^{gfp/gfp}), B6.129S7-Ifng^{tm1Ts}/J (IFN^{-/-}), and B6;129S-Tnf^{tm1Gkl}/J (TNFa^{-/-}) mice were purchased from the Jackson Laboratory and either used or bred in house. F1 crosses were made between CX3CR1-Cre-ER and ROSA Stop^{fl/fl} DTR mice as well as B6 and CX3CR1^{gfp/gfp} mice. H-2K^bD^b^{-/-} (**96**), IFNAR^{-/-} (**32**) (provided by Jonathan Sprent, formerly at The Scripps Research Institute), P14 (**37**), OFP⁺ P14 (**97**), mTomato⁺ P14, mTomato⁺ GCaMP6s⁺ P14, mCerulean⁺ OT-I (**97**), mTomato⁺ OT-I, CD45.1, and actin-GCaMP6s mTomato OT-I (**13**) and were bred and maintained under specific pathogen-free conditions at the National Institutes of Health (NIH). OMP-GFP (**98**) mice were provided by Leo Belluscio, NINDS, and backcrossed onto a C57BL/6J background. All mice in this study were handled in accordance with the guidelines set forth by the NIH Animal Care and Use Committee.

Viruses and plaque assays

LCMV, VSV-OVA serotype Indiana (provided by Leo Lefrancois, formerly at the University of Connecticut) (**99**), VSV-eGFP (**100**), VSV-DsRed, VSV-iCre, and VSV-PeGFP (**48**) were propagated on BHK21 cells. Infectivity of VSV preparations was quantified by plaque assay on green monkey kidney cells (Vero). VSV titers from brains of infected mice were determined similarly. Briefly, animals were perfused with saline, brains were immersed in 1 ml of 2% FBS RPMI containing zirconia silica beads and homogenized with a FastPrep 24-5G (MP Biomedical). Homogenates were spun for 3 min at 15,000g, and supernatants were serially diluted for quantification on Vero cells. One-hundred microliters of diluted homogenate was added to Vero monolayers in flat bottom 24-well plates and incubated for ~3 hours. One-hundred microliters of 0.75% methylcellulose in DMEM (containing 10% FBS, 1% glutamine, and 1% Pen/Strep) were added to each well and incubated for

(pFL-VSV-Ova-IRES-iCre) flanked by BsiWI site at G-L junction of the plasmid. The recombinant VSV expressing OVA and iCre recombinase was recovered by co-transfection of full-length plasmids along with supporting plasmids pN, pP, and pL (carrying the coding sequences of the N, P, and L proteins of VSV) in BHK-21 cells as per the protocol published earlier (48). The recombinant virus (rVSV-OVA-iCre) was plaque purified and viral stocks were prepared using BHK-21 cells. Lastly, a Western blot was performed to confirm expression of Ova and iCre proteins in cell lysates from BHK-21 cells infected with rVSV-OVA-iCre.

Infections

Eight- to 10-week-old mice were infected intranasally by injecting 10 μ L of viral diluent in each nostril. For survival, titering, immunohistochemical, flow cytometric, and microarray experiments, mice were infected with 1×10^5 PFU of VSV per nostril. For intravital imaging experiments, mice were infected with 4×10^5 PFU per nostril to ensure more uniform OB infection. For experiments involving LCMV, mice were infected i.p. with 2×10^5 PFU of LCMV Armstrong.

Transgenic mouse generation

Floxed beta-2 microglobulin (β 2M) knock-in mice (floxed β 2M) were generated by Cyagen Biosciences. Homology arms were derived from BAC clones RP23-285J7 and RP23-299B11 from the C57BL/6 library and LoxP sites were inserted into genomic positions flanking exons 2 and 3 of the beta microglobulin gene (fig. S4). Homologous recombination was performed in C57BL/6 ES cells before transfer into C57BL/6 embryos. Positive founder lines were backcrossed one additional generation onto the C57BL/6J background before intercrossing.

SUPPLEMENTARY MATERIALS

immunology.sciencemag.org/cgi/content/full/5/48/eabb1817/DC1

Materials and Methods

Fig. S1. Diagrams of sectioning planes through the mouse head.

Fig. S2. Parenchymal cells within the OB and brain survive VSV infection after intranasal inoculation.

Fig. S3. Virus-specific CTLs flux calcium for longer durations while undergoing stable interactions.

Fig. S4. Generation of floxed β 2M transgenic mice.

outer nerve layer.

Movie S2. Virus-specific CTLs survey the infected glomerular layer with the OB.

Movie S3. Antiviral CTLs engage cognate antigen and flux calcium within the infected OB.

Movie S4. Antiviral CTLs flux calcium upon contact with microglia.

References ([102](#), [103](#))

[View/request a protocol for this paper from Bio-protocol.](#)

<http://www.sciencemag.org/about/science-licenses-journal-article-reuse>

This is an article distributed under the terms of the [Science Journals Default License](#).

REFERENCES AND NOTES

1. ↪ P. A. Swanson II., D. B. McGavern, Viral diseases of the central nervous system. *Curr. Opin. Virol.* **11**, 44–54 (2015). [OpenUrl](#) [CrossRef](#) [PubMed](#)
2. ↪ K. L. Tyler, Acute Viral Encephalitis. *N. Engl. J. Med.* **379**, 557–566 (2018). [OpenUrl](#)
3. ↪ J. V. Forrester, P. G. McMenamin, S. J. Dando, CNS infection and immune privilege. *Nat. Rev. Neurosci.* **19**, 655–671 (2018). [OpenUrl](#) [CrossRef](#)
4. ↪ D. B. McGavern, S. S. Kang, Illuminating viral infections in the nervous system. *Nat. Rev. Immunol.* **11**, 318–329 (2011). [OpenUrl](#) [CrossRef](#) [PubMed](#)
5. ↪ A. W. Barrios, G. Nunez, P. Sanchez Quinteiro, I. Salazar, Anatomy, histochemistry, and immunohistochemistry of the olfactory subsystems in mice. *Front. Neuroanat.* **8**, 63 (2014). [OpenUrl](#)
6. ↪ D. van Riel, R. Verdijk, T. Kuiken, The olfactory nerve: A shortcut for influenza and other viral diseases into the central nervous system. *J. Pathol.* **235**, 277–287 (2015). [OpenUrl](#) [CrossRef](#) [PubMed](#)
7. ↪ I. Mori, Y. Nishiyama, T. Yokochi, Y. Kimura, Olfactory transmission of neurotropic viruses. *J. Neurovirol.* **11**, 129–137 (2005). [OpenUrl](#) [CrossRef](#) [PubMed](#) [Web of Science](#)
8. ↪ G. K. Binder, D. E. Griffin, Interferon-gamma-mediated site-specific clearance of alphavirus from CNS neurons. *Science* **293**, 303–306 (2001). [OpenUrl](#) [Abstract/FREE Full Text](#)

2297–2304 (2009). [OpenUrl](#) [Abstract/FREE Full Text](#)

11. ↵ F. McNab, K. Mayer-Barber, A. Sher, A. Wack, A. O'Garra, Type I interferons in infectious disease. *Nat. Rev. Immunol.* **15**, 87–103 (2015). [OpenUrl](#) [CrossRef](#) [PubMed](#)
12. ↵ J. Crouse, U. Kalinke, A. Oxenius, Regulation of antiviral T cell responses by type I interferons. *Nat. Rev. Immunol.* **15**, 231–242 (2015). [OpenUrl](#) [CrossRef](#) [PubMed](#)
13. ↵ E. A. Moseman, T. Wu, J. C. de la Torre, P. L. Schwartzberg, D. B. McGavern, Type I interferon suppresses virus-specific B cell responses by modulating CD8⁺ T cell differentiation. *Sci. Immunol.* **1**, eaah3565 (2016). [OpenUrl](#) [Abstract/FREE Full Text](#)
14. ↵ C. E. Patterson, D. M. P. Lawrence, L. A. Echols, G. F. Rall, Immune-mediated protection from measles virus-induced central nervous system disease is noncytolytic and gamma interferon dependent. *J. Virol.* **76**, 4497–4506 (2002). [OpenUrl](#) [Abstract/FREE Full Text](#)
15. A. Tishon, H. Lewicki, A. Andaya, D. McGavern, L. Martin, M. B. A. Oldstone, CD4 T cell control primary measles virus infection of the CNS: Regulation is dependent on combined activity with either CD8 T cells or with B cells: CD4, CD8 or B cells alone are ineffective. *Virology* **347**, 234–245 (2006). [OpenUrl](#) [CrossRef](#) [PubMed](#) [Web of Science](#)
16. ↵ T. Liu, K. M. Khanna, B. N. Carriere, R. L. Hendricks, Gamma interferon can prevent herpes simplex virus type 1 reactivation from latency in sensory neurons. *J. Virol.* **75**, 11178–11184 (2001). [OpenUrl](#) [Abstract/FREE Full Text](#)
17. ↵ E. M. Cantin, D. R. Hinton, J. Chen, H. Openshaw, Gamma interferon expression during acute and latent nervous system infection by herpes simplex virus type 1. *J. Virol.* **69**, 4898–4905 (1995). [OpenUrl](#) [Abstract/FREE Full Text](#)
18. ↵ L. G. Guidotti, F. V. Chisari, Noncytolytic control of viral infections by the innate and adaptive immune response. *Annu. Rev. Immunol.* **19**, 65–91 (2001). [OpenUrl](#) [CrossRef](#) [PubMed](#) [Web of Science](#)
19. ↵ P. N. Gilles, G. Fey, F. V. Chisari, Tumor necrosis factor alpha negatively regulates hepatitis B virus gene expression in transgenic mice. *J. Virol.* **66**, 3955–3960 (1992). [OpenUrl](#) [Abstract/FREE Full Text](#)
20. ↵ H. Lauterbach, E. I. Zuniga, P. Truong, M. B. Oldstone, D. B. McGavern, Adoptive immunotherapy induces CNS dendritic cell recruitment and antigen presentation during clearance of a persistent viral infection. *J. Exp. Med.* **203**, 1963–1975 (2006). [OpenUrl](#) [Abstract/FREE Full Text](#)
21. ↵ B. Lundh, K. Kristensson, E. Norrby, Selective infections of olfactory and respiratory epithelium by vesicular stomatitis and Sendai viruses. *Neuropathol. Appl. Neurobiol.* **13**, 111–122 (1987). [OpenUrl](#) [CrossRef](#) [PubMed](#) [Web of Science](#)

[Web of Science](#)

24. ↪ I. Mori, T. Komatsu, K. Takeuchi, K. Nakakuki, M. Sudo, Y. Kimura, Parainfluenza virus type 1 infects olfactory neurons and establishes long-term persistence in the nerve tissue. *J. Gen. Virol.* **76**, 1251–1254 (1995). [OpenUrl](#) [CrossRef](#) [PubMed](#) [Web of Science](#)
25. ↪ S. L. Park, Y.-J. S. Huang, A. C. Lyons, V. B. Ayers, S. M. Hettenbach, D. S. McVey, K. R. Burton, S. Higgs, D. L. Vanlandingham, North American domestic pigs are susceptible to experimental infection with Japanese encephalitis virus. *Sci. Rep.* **8**, 7951 (2018). [OpenUrl](#) [CrossRef](#)
26. ↪ I. Mori, F. Goshima, Y. Imai, S. Kohsaka, T. Sugiyama, T. Yoshida, T. Yokochi, Y. Nishiyama, Y. Kimura, Olfactory receptor neurons prevent dissemination of neurovirulent influenza A virus into the brain by undergoing virus-induced apoptosis. *J. Gen. Virol.* **83**, 2109–2116 (2002). [OpenUrl](#) [CrossRef](#) [PubMed](#)
[Web of Science](#)
27. ↪ J. M. van den Brand, K. J. Stittelaar, G. van Amerongen, L. Reperant, L. de Waal, A. D. Osterhaus, T. Kuiken, Comparison of temporal and spatial dynamics of seasonal H3N2, pandemic H1N1 and highly pathogenic avian influenza H5N1 virus infections in ferrets. *PLOS ONE* **7**, e42343 (2012). [OpenUrl](#) [CrossRef](#)
[PubMed](#)
28. ↪ E. J. Schrauwen, S. Herfst, L. M. Leijten, P. van Run, T. M. Bestebroer, M. Linster, R. Bodewes, J. H. Kreijtz, G. F. Rimmelzwaan, A. D. Osterhaus, R. A. Fouchier, T. Kuiken, D. van Riel, The multibasic cleavage site in H5N1 virus is critical for systemic spread along the olfactory and hematogenous routes in ferrets. *J. Virol.* **86**, 3975–3984 (2012). [OpenUrl](#) [Abstract/FREE Full Text](#)
29. ↪ B. S. Huneycutt, Z. Bi, C. J. Aoki, C. S. Reiss, Central neuropathogenesis of vesicular stomatitis virus infection of immunodeficient mice. *J. Virol.* **67**, 6698–6706 (1993). [OpenUrl](#) [Abstract/FREE Full Text](#)
30. ↪ C. S. Reiss, I. V. Plakhov, T. Komatsu, Viral replication in olfactory receptor neurons and entry into the olfactory bulb and brain. *Ann. N. Y. Acad. Sci.* **855**, 751–761 (1998). [OpenUrl](#) [CrossRef](#) [PubMed](#)
31. ↪ T. E. Cornish, D. E. Stallknecht, C. C. Brown, B. S. Seal, E. W. Howerth, Pathogenesis of experimental vesicular stomatitis virus (New Jersey serotype) infection in the deer mouse (*Peromyscus maniculatus*). *Vet. Pathol.* **38**, 396–406 (2001). [OpenUrl](#) [CrossRef](#) [PubMed](#) [Web of Science](#)
32. ↪ U. Müller, U. Steinhoff, L. F. Reis, S. Hemmi, J. Pavlovic, R. M. Zinkernagel, M. Aguet, Functional role of type I and type II interferons in antiviral defense. *Science* **264**, 1918–1921 (1994). [OpenUrl](#)
[Abstract/FREE Full Text](#)
33. ↪ U. Steinhoff, U. Müller, A. Schertler, H. Hengartner, M. Aguet, R. M. Zinkernagel, Antiviral protection by vesicular stomatitis virus-specific antibodies in alpha/beta interferon receptor-deficient mice. *J. Virol.* **69**, 2153–2158 (1995). [OpenUrl](#) [Abstract/FREE Full Text](#)

36. ↪ D. E. Griffin, T. Metcalf, Clearance of virus infection from the CNS. *Curr. Opin. Immunol.* **1**, 216–221 (2011). [OpenUrl](#)
37. ↪ H. Pircher, K. Bürki, R. Lang, H. Hengartner, R. M. Zinkernagel, Tolerance induction in double specific T-cell receptor transgenic mice varies with antigen. *Nature* **342**, 559–561 (1989). [OpenUrl](#) [CrossRef](#) [PubMed](#) [Web of Science](#)
38. ↪ G. Yang, F. Pan, C. N. Parkhurst, J. Grutzendler, W.-B. Gan, Thinned-skull cranial window technique for long-term imaging of the cortex in live mice. *Nat. Protoc.* **5**, 201–208 (2010). [OpenUrl](#) [CrossRef](#) [PubMed](#) [Web of Science](#)
39. ↪ M. Manglani, D. B. McGavern, Intravital imaging of neuroimmune interactions through a thinned skull. *Curr. Protoc. Immunol.* **120**, 24.2.21–24.2.12 (2018). [OpenUrl](#)
40. ↪ H. D. Moreau, F. Lemaître, K. R. Garrod, Z. Garcia, A.-M. Lennon-Dumenil, P. Bousso, Signal strength regulates antigen-mediated T-cell deceleration by distinct mechanisms to promote local exploration or arrest. *Proc. Natl. Acad. Sci. U.S.A.* **112**, 12151–12156 (2015). [OpenUrl](#) [Abstract/FREE Full Text](#)
41. ↪ M. Oh-hora, A. Rao, Calcium signaling in lymphocytes. *Curr. Opin. Immunol.* **20**, 250–258 (2008). [OpenUrl](#) [CrossRef](#) [PubMed](#) [Web of Science](#)
42. ↪ D. R. Fooksman, S. Vardhana, G. Vasiliver-Shamis, J. Liese, D. A. Blair, J. Waite, C. Sacristán, G. D. Victora, A. Zanin-Zhorov, M. L. Dustin, Functional anatomy of T cell activation and synapse formation. *Annu. Rev. Immunol.* **28**, 79–105 (2010). [OpenUrl](#) [CrossRef](#) [PubMed](#) [Web of Science](#)
43. ↪ E. Joly, L. Mucke, M. B. Oldstone, Viral persistence in neurons explained by lack of major histocompatibility class I expression. *Science* **253**, 1283–1285 (1991). [OpenUrl](#) [Abstract/FREE Full Text](#)
44. ↪ E. Joly, M. B. Oldstone, Neuronal cells are deficient in loading peptides onto MHC class I molecules. *Neuron* **8**, 1185–1190 (1992). [OpenUrl](#) [CrossRef](#) [PubMed](#) [Web of Science](#)
45. ↪ B. H. Koller, P. Marrack, J. W. Kappler, O. Smithies, Normal development of mice deficient in beta 2M, MHC class I proteins, and CD8⁺ T cells. *Science* **248**, 1227–1230 (1990). [OpenUrl](#) [Abstract/FREE Full Text](#)
46. ↪ D. Nayak, T. L. Roth, D. B. McGavern, Microglia development and function. *Annu. Rev. Immunol.* **32**, 367–402 (2014). [OpenUrl](#) [CrossRef](#) [PubMed](#) [Web of Science](#)
47. ↪ F. W. van Ginkel, R. J. Jackson, Y. Yuki, J. R. McGhee, Cutting edge: The mucosal adjuvant cholera toxin redirects vaccine proteins into olfactory tissues. *J. Immunol.* **165**, 4778–4782 (2000). [OpenUrl](#) [Abstract/FREE Full Text](#)
48. ↪ S. C. Das, D. Nayak, Y. Zhou, A. K. Pattnaik, Visualization of intracellular transport of vesicular stomatitis virus nucleocapsids in living cells. *J. Virol.* **80**, 6368–6377 (2006). [OpenUrl](#) [Abstract/FREE Full Text](#)

microglia viability, unmasking a microglia progenitor cell in the adult brain. *Neuron* **82**, 380–397 (2014).

[OpenUrl](#) [CrossRef](#) [PubMed](#) [Web of Science](#)

51. ↵ Z. Bi, M. Barna, T. Komatsu, C. S. Reiss, Vesicular stomatitis virus infection of the central nervous system activates both innate and acquired immunity. *J. Virol.* **69**, 6466–6472 (1995). [OpenUrl](#) [Abstract/FREE Full Text](#)
52. Z. Bi, C. S. Reiss, Inhibition of vesicular stomatitis virus infection by nitric oxide. *J. Virol.* **69**, 2208–2213 (1995). [OpenUrl](#) [Abstract/FREE Full Text](#)
53. T. Komatsu, D. D. Ireland, N. Chen, C. S. Reiss, Neuronal expression of NOS-1 is required for host recovery from viral encephalitis. *Virology* **258**, 389–395 (1999). [OpenUrl](#) [CrossRef](#) [PubMed](#) [Web of Science](#)
54. T. Komatsu, Z. Bi, C. S. Reiss, Interferon- γ induced type I nitric oxide synthase activity inhibits viral replication in neurons. *J. Neuroimmunol.* **68**, 101–108 (1996). [OpenUrl](#) [CrossRef](#) [PubMed](#) [Web of Science](#)
55. ↵ T. Komatsu, M. Barna, C. S. Reiss, Interleukin-12 promotes recovery from viral encephalitis. *Viral Immunol.* **10**, 35–47 (1997). [OpenUrl](#) [CrossRef](#) [PubMed](#)
56. ↵ C. T. Leung, P. A. Coulombe, R. R. Reed, Contribution of olfactory neural stem cells to tissue maintenance and regeneration. *Nat. Neurosci.* **10**, 720–726 (2007). [OpenUrl](#) [CrossRef](#) [PubMed](#) [Web of Science](#)
57. ↵ J. E. Schwob, Neural regeneration and the peripheral olfactory system. *Anat. Rec.* **269**, 33–49 (2002). [OpenUrl](#) [CrossRef](#) [PubMed](#)
58. ↵ L. G. Guidotti, F. V. Chisari, Cytokine-induced viral purging--role in viral pathogenesis. *Curr. Opin. Microbiol.* **2**, 388–391 (1999). [OpenUrl](#) [CrossRef](#) [PubMed](#) [Web of Science](#)
59. ↵ L. G. Guidotti, R. Rochford, J. Chung, M. Shapiro, R. Purcell, F. V. Chisari, Viral clearance without destruction of infected cells during acute HBV infection. *Science* **284**, 825–829 (1999). [OpenUrl](#) [Abstract/FREE Full Text](#)
60. ↵ L. G. Guidotti, P. Borrow, A. Brown, H. McClary, R. Koch, F. V. Chisari, Noncytopathic clearance of lymphocytic choriomeningitis virus from the hepatocyte. *J. Exp. Med.* **189**, 1555–1564 (1999). [OpenUrl](#) [Abstract/FREE Full Text](#)
61. ↵ J. Herz, K. R. Johnson, D. B. McGavern, Therapeutic antiviral T cells noncytopathically clear persistently infected microglia after conversion into antigen-presenting cells. *J. Exp. Med.* **212**, 1153–1169 (2015). [OpenUrl](#) [Abstract/FREE Full Text](#)
62. ↵ N. S. Heaton, R. A. Langlois, D. Sachs, J. K. Lim, P. Palese, B. R. tenOever, Long-term survival of influenza virus infected club cells drives immunopathology. *J. Exp. Med.* **211**, 1707–1714 (2014). [OpenUrl](#) [Abstract/FREE Full Text](#)

65. ↪ R. Burdeinick-Kerr, D. E. Griffin, Gamma interferon-dependent, noncytolytic clearance of sindbis virus infection from neurons in vitro. *J. Virol.* **79**, 5374–5385 (2005). [OpenUrl](#) [Abstract/FREE Full Text](#)
66. ↪ G. Faulkner, M. Dubois-Dalcq, E. Hooghe-Peters, H. F. McFarland, R. A. Lazzarini, Defective interfering particles modulate VSV infection of dissociated neuron cultures. *Cell* **17**, 979–991 (1979). [OpenUrl](#) [CrossRef](#) [PubMed](#)
67. ↪ B. D. Pearce, M. V. Hobbs, T. S. McGraw, M. J. Buchmeier, Cytokine induction during T-cell-mediated clearance of mouse hepatitis virus from neurons in vivo. *J. Virol.* **68**, 5483–5495 (1994). [OpenUrl](#) [Abstract/FREE Full Text](#)
68. ↪ J. Hausmann, A. Pagenstecher, K. Baur, K. Richter, H.-J. Rziha, P. Staeheli, CD8 T cells require gamma interferon to clear borna disease virus from the brain and prevent immune system-mediated neuronal damage. *J. Virol.* **79**, 13509–13518 (2005). [OpenUrl](#) [Abstract/FREE Full Text](#)
69. ↪ T. M. Kündig, H. Hengartner, R. M. Zinkernagel, T cell-dependent IFN-gamma exerts an antiviral effect in the central nervous system but not in peripheral solid organs. *J. Immunol.* **150**, 2316–2321 (1993). [OpenUrl](#) [Abstract/FREE Full Text](#)
70. ↪ B. Shrestha, B. Zhang, W. E. Purtha, R. S. Klein, M. S. Diamond, Tumor necrosis factor alpha protects against lethal West Nile virus infection by promoting trafficking of mononuclear leukocytes into the central nervous system. *J. Virol.* **82**, 8956–8964 (2008). [OpenUrl](#) [Abstract/FREE Full Text](#)
71. ↪ D. Hayasaka, K. Shirai, K. Aoki, N. Nagata, D. S. Simantini, K. Kitaura, Y. Takamatsu, E. Gould, R. Suzuki, K. Morita, TNF- α acts as an immunoregulator in the mouse brain by reducing the incidence of severe disease following Japanese encephalitis virus infection. *PLOS ONE* **8**, e71643 (2013). [OpenUrl](#) [CrossRef](#) [PubMed](#)
72. ↪ M. M. Tun, K. Aoki, M. Senba, C. C. Buerano, K. Shirai, R. Suzuki, K. Morita, D. Hayasaka, Protective role of TNF- α , IL-10 and IL-2 in mice infected with the Oshima strain of Tick-borne encephalitis virus. *Sci. Rep.* **4**, 5344 (2014). [OpenUrl](#) [CrossRef](#) [PubMed](#)
73. ↪ Y. Sergerie, S. Rivest, G. Boivin, Tumor necrosis factor- α and interleukin-1 β play a critical role in the resistance against lethal herpes simplex virus encephalitis. *J. Infect. Dis.* **196**, 853–860 (2007). [OpenUrl](#) [CrossRef](#) [PubMed](#) [Web of Science](#)
74. ↪ X. Zhang, D. R. Hinton, D. J. Cua, S. A. Stohlman, M. M. Lai, Expression of interferon- γ by a coronavirus defective-interfering RNA vector and its effect on viral replication, spread, and pathogenicity. *Virology* **233**, 327–338 (1997). [OpenUrl](#) [CrossRef](#) [PubMed](#)
75. M. T. Liu, D. Armstrong, T. A. Hamilton, T. E. Lane, Expression of Mig (monokine induced by interferon- γ) is important in T lymphocyte recruitment and host defense following viral infection of the central nervous system. *J. Immunol.* **166**, 1790–1795 (2001). [OpenUrl](#) [Abstract/FREE Full Text](#)

[Abstract/FREE Full Text](#)

78. ↪ B. M. Elmer, A. K. McAllister, Major histocompatibility complex class I proteins in brain development and plasticity. *Trends Neurosci.* **35**, 660–670 (2012). [OpenUrl](#) [CrossRef](#) [PubMed](#) [Web of Science](#)
79. ↪ G. F. Rall, CNS neurons: The basis and benefits of low class I major histocompatibility complex expression. *Curr. Top. Microbiol. Immunol.* **232**, 115–134 (1998). [OpenUrl](#) [PubMed](#) [Web of Science](#)
80. ↪ G. Chevalier, E. Suberbielle, C. Monnet, V. Duplan, G. Martin-Blondel, F. Farrugia, G. Le Masson, R. Liblau, D. Gonzalez-Dunia, Neurons are MHC class I-dependent targets for CD8 T cells upon neurotropic viral infection. *PLOS Pathog.* **7**, e1002393 (2011). [OpenUrl](#) [CrossRef](#) [PubMed](#)
81. ↪ T. Liu, K. M. Khanna, X. Chen, D. J. Fink, R. L. Hendricks, CD8⁺ T cells can block herpes simplex virus type 1 (HSV-1) reactivation from latency in sensory neurons. *J. Exp. Med.* **191**, 1459–1466 (2000). [OpenUrl](#)
[Abstract/FREE Full Text](#)
82. ↪ J. E. Knickelbein, K. M. Khanna, M. B. Yee, C. J. Baty, P. R. Kinchington, R. L. Hendricks, Noncytotoxic lytic granule-mediated CD8⁺ T cell inhibition of HSV-1 reactivation from neuronal latency. *Science* **322**, 268–271 (2008). [OpenUrl](#) [Abstract/FREE Full Text](#)
83. ↪ B. Shrestha, M. A. Samuel, M. S. Diamond, CD8⁺ T cells require perforin to clear West Nile virus from infected neurons. *J. Virol.* **80**, 119–129 (2006). [OpenUrl](#) [Abstract/FREE Full Text](#)
84. ↪ F. M. Cruz, J. D. Colbert, E. Merino, B. A. Kriegsmann, K. L. Rock, The biology and underlying mechanisms of cross-presentation of exogenous antigens on MHC-I molecules. *Annu. Rev. Immunol.* **35**, 149–176 (2017). [OpenUrl](#) [CrossRef](#) [PubMed](#)
85. ↪ C. Beauvillain, S. Donnou, U. Jarry, M. Scotet, H. Gascan, Y. Delneste, P. Gueronprez, P. Jeannin, D. Couez, Neonatal and adult microglia cross-present exogenous antigens. *Glia* **56**, 69–77 (2008). [OpenUrl](#)
[PubMed](#)
86. ↪ M. J. Vasek, C. Garber, D. Dorsey, D. M. Durrant, B. Bollman, A. Soung, J. Yu, C. Perez-Torres, A. Frouin, D. K. Wilton, K. Funk, B. K. DeMasters, X. Jiang, J. R. Bowen, S. Mennerick, J. K. Robinson, J. R. Garbow, K. L. Tyler, M. S. Suthar, R. E. Schmidt, B. Stevens, R. S. Klein, A complement-microglial axis drives synapse loss during virus-induced memory impairment. *Nature* **534**, 538–543 (2016). [OpenUrl](#)
[CrossRef](#) [PubMed](#)
87. ↪ S. Seitz, P. Clarke, K. L. Tyler, Pharmacologic depletion of microglia increases viral load in the brain and enhances mortality in murine models of flavivirus-induced encephalitis. *J. Virol.* **92**, e00525–e00518 (2018).
[OpenUrl](#)
88. ↪ R. Fekete, C. Cserép, N. Lénárt, K. Tóth, B. Orsolits, B. Martinecz, E. Méhes, B. Szabó, V. Németh, B. Gönci, B. Sperlágh, Z. Boldogkői, Á. Kittel, M. Baranyi, S. Ferenczi, K. Kovács, G. Szalay, B. Rózsa, C. Webb, G. G. Kovacs, T. Hortobágyi, B. L. West, Z. Környei, Á. Dénes, Microglia control the spread of

90. ↪ I. Waltl, C. Käuter, I. Gerhauser, C. Chhatbar, L. Ghita, U. Kalinke, W. Löscher, Microglia have a protective role in viral encephalitis-induced seizure development and hippocampal damage. *Brain Behav. Immun.* **74**, 186–204 (2018). [OpenUrl](#) [CrossRef](#) [PubMed](#)
91. ↪ C. Chhatbar, C. N. Detje, E. Grabski, K. Borst, J. Spanier, L. Ghita, D. A. Elliott, M. J. C. Jordão, N. Mueller, J. Sutton, C. K. Prajeeth, V. Gudi, M. A. Klein, M. Prinz, F. Bradke, M. Stangel, U. Kalinke, Type I interferon receptor signaling of neurons and astrocytes regulates microglia activation during viral encephalitis. *Cell Rep.* **25**, 118–129.e4 (2018). [OpenUrl](#) [CrossRef](#) [PubMed](#)
92. ↪ K. E. Funk, R. S. Klein, CSF1R antagonism limits local restimulation of antiviral CD8⁺ T cells during viral encephalitis. *J. Neuroinflammation* **16**, 22 (2019). [OpenUrl](#)
93. ↪ C. Garber, A. Soung, L. L. Vollmer, M. Kanmogne, A. Last, J. Brown, R. S. Klein, T cells promote microglia-mediated synaptic elimination and cognitive dysfunction during recovery from neuropathogenic flaviviruses. *Nat. Neurosci.* **22**, 1276–1288 (2019). [OpenUrl](#)
94. ↪ P. M. D'Agostino, C. Kwak, H. A. Vecchiarelli, J. G. Toth, J. M. Miller, Z. Masheeb, B. S. McEwen, K. Bulloch, Viral-induced encephalitis initiates distinct and functional CD103⁺ CD11b⁺ brain dendritic cell populations within the olfactory bulb. *Proc. Natl. Acad. Sci. U.S.A.* **109**, 6175–6180 (2012). [OpenUrl](#)
[Abstract/FREE Full Text](#)
95. ↪ M. D. Bern, B. A. Parikh, L. Yang, D. L. Beckman, J. Poursine-Laurent, W. M. Yokoyama, Inducible down-regulation of MHC class I results in natural killer cell tolerance. *J. Exp. Med.* **216**, 99–116 (2019). [OpenUrl](#)
[Abstract/FREE Full Text](#)
96. ↪ B. Pérarnau, M. F. Saron, B. R. San Martin, N. Bervas, H. Ong, M. J. Soloski, A. G. Smith, J. M. Ure, J. E. Gairin, F. A. Lemonnier, Single *H2K^b*, *H2D^b* and double *H2K^bD^b* knockout mice: Peripheral CD8⁺ T cell repertoire and anti-lymphocytic choriomeningitis virus cytolytic responses. *Eur. J. Immunol.* **29**, 1243–1252 (1999). [OpenUrl](#) [CrossRef](#) [PubMed](#) [Web of Science](#)
97. ↪ S. Gossa, D. Nayak, B. H. Zinselmeyer, D. B. McGavern, Development of an immunologically tolerated combination of fluorescent proteins for *in vivo* two-photon imaging. *Sci. Rep.* **4**, 6664 (2014). [OpenUrl](#)
[CrossRef](#) [PubMed](#)
98. ↪ S. M. Potter, C. Zheng, D. S. Koos, P. Feinstein, S. E. Fraser, P. Mombaerts, Structure and emergence of specific olfactory glomeruli in the mouse. *J. Neurosci.* **21**, 9713–9723 (2001). [OpenUrl](#) [Abstract/FREE Full Text](#)
99. ↪ S. K. Kim, D. S. Reed, S. Olson, M. J. Schnell, J. K. Rose, P. A. Morton, L. Lefrançois, Generation of mucosal cytotoxic T cells against soluble protein by tissue-specific environmental and costimulatory signals. *Proc. Natl. Acad. Sci. U.S.A.* **95**, 10814–10819 (1998). [OpenUrl](#) [Abstract/FREE Full Text](#)
100. ↪ K. Chandran, N. J. Sullivan, U. Felbor, S. P. Whelan, J. M. Cunningham, Endosomal proteolysis of the Ebola virus glycoprotein is necessary for infection. *Science* **308**, 1643–1645 (2005). [OpenUrl](#)
[Abstract/FREE Full Text](#)

(2009). [OpenUrl](#) [CrossRef](#) [PubMed](#)

103. ↵ E. A. Susaki, K. Tainaka, D. Perrin, H. Yukinaga, A. Kuno, H. R. Ueda, Advanced CUBIC protocols for whole-brain and whole-body clearing and imaging. *Nat. Protoc.* **10**, 1709–1727 (2015). [OpenUrl](#) [CrossRef](#) [PubMed](#)

Acknowledgments: We thank A. Hoofring in the NIH Medical Arts Design Section for generating the illustration shown in fig. S1. **Funding:** This research was supported by the intramural program at the NIH. **Author contributions:** A.C.B. and E.A.M. performed all the experiments and analyzed data. D.N. generated VSV recombinants. D.B.M. provided the funding. E.A.M. and D.B.M. wrote the manuscript. **Competing interests:** The authors declare that they have no competing interests. **Data and materials availability:** All data needed to evaluate the conclusions are present in the paper or the Supplementary Materials.

Copyright © 2020 The Authors, some rights reserved; exclusive licensee American Association for the Advancement of Science. No claim to original U.S. Government Works

View Abstract

Recommended articles from TrendMD

Processing by Caspases

John F. Foley, *Sci Signal*, 2010

Absence of MHC class II on cDC1 dendritic cells triggers fatal autoimmunity to a cross-presented self-antigen

Christian Wohn et al., *Sci Immunol*, 2020

Enzymatic synthesis of core 2 O-glycans governs the tissue-trafficking potential of memory CD8+ T cells

Jossef F. Osborn et al., *Sci Immunol*, 2017

Constitutive resistance to viral infection in human CD141+ dendritic cells

Amyeric Silvin et al., *Sci Immunol*, 2017

Up-regulation of LFA-1 allows liver-resident memory T cells to patrol and remain in the hepatic sinusoids

H. A. McNamara et al., *Sci Immunol*, 2017

Peptide splicing by the proteasome

Nathalie Vigneron et al., *Journal of Biological Chemistry*, 2017

Are the mechanisms involved in astrocyte and lymphocyte death during HIV infection similar?

Diego S Ojeda et al., *Neural Regeneration Research*, 2019

The viability of co-active fuzzy inference system model for monthly reference evapotranspiration estimation: case study of Uttarakhand State

Malik et al., *Hydrology Research*, 2019

Attenuated plasmodium sporozoite expressing MAGE-A3 induces antigen-specific CD8+ T cell response against lung cancer in mice

Dong Zhou et al., *Cancer Biology & Medicine*, 2019

The plasticity of plasticity: lesson from remote microglia induced by focal central nervous system injury

Strategic Contributor



Science Immunology

Vol 5, Issue 48
12 June 2020

[Table of Contents](#)

ARTICLE TOOLS

 [Email](#)

 [Print](#)

 [Alerts](#)

 [Share](#)

 [Download Powerpoint](#)

 [Citation tools](#)

MY SAVED FOLDERS

 [Save to my folders](#)

STAY CONNECTED TO SCIENCE IMMUNOLOGY

- [Facebook](#)
- [Twitter](#)

RELATED CONTENT

Vol. 368, Issues 6-10



[Table of Contents](#)

SOCIAL SCIENCE: COVID-19

Which interventions work best in a pandemic?

ECOLOGY

Colonialism and its consequences

SCI COMMUN

News at a glance

ECOLOGY

Blue carbon from the past forecasts the future

WORKING LIFE

No place like home

About Us

- [Journals](#)
- [News from Science](#)
- [Leadership](#)
- [Team Members](#)
- [Work at AAAS](#)

For Advertisers

- [Advertising Kits](#)
- [Awards and Prizes](#)
- [Custom Publishing](#)
- [Webinars](#)

For Authors

- [Submit](#)
- [Information for Authors](#)
- [Editorial Policies](#)

For Librarians

- [Manage Your Institutional Subscription](#)
- [Information for Librarians](#)
- [Request a Quote](#)
- [FAQs](#)

Related Jobs

Postdoctoral Appointee in Optical Artificial Intelligence

Sandia National Laboratories
Livermore, California

School of Optical-Electrical and Computer Engineering of USST Invites Global Talents


University of Shanghai for Science and Technology
Shanghai (CN)

Chair, Department of Physics

Southern University of Science and Technology (SUSTech)
Shenzhen, China

[MORE JOBS ►](#)

NAVIGATE THIS ARTICLE

- Article
 - Safeguarding the sense of smell
 - Abstract
 - INTRODUCTION
 - RESULTS
 - DISCUSSION
 - MATERIALS AND METHODS
 - SUPPLEMENTARY MATERIALS
 - REFERENCES AND NOTES
- Figures & Data
- Info & Metrics
- eLetters
-  PDF

Help

[Access and Subscriptions](#)

[Order a Single Issue](#)

[Reprints and Permissions](#)

[Contact Us](#)

[Accessibility](#)

Stay Connected



© 2020 American Association for the Advancement of Science. All rights reserved. AAAS is a partner of HINARI, AGORA, OARE, CHORUS, CLOCKSS, CrossRef and COUNTER.
Science Immunology ISSN 2470-9468.

[Terms of Service](#)

[Privacy Policy](#)

[Contact AAAS](#)